

## Analytically estimating the efficiency of high temperature aquifer thermal energy storage

Geerts, David; Daniilidis, Alexandros; Kramer, Gert Jan; Bloemendal, Martin; Liu, Wen

**DOI**

[10.1186/s40517-025-00343-8](https://doi.org/10.1186/s40517-025-00343-8)

**Publication date**

2025

**Document Version**

Final published version

**Published in**

Geothermal Energy

**Citation (APA)**

Geerts, D., Daniilidis, A., Kramer, G. J., Bloemendal, M., & Liu, W. (2025). Analytically estimating the efficiency of high temperature aquifer thermal energy storage. *Geothermal Energy*, 13(17).  
<https://doi.org/10.1186/s40517-025-00343-8>

**Important note**

To cite this publication, please use the final published version (if applicable).  
Please check the document version above.

**Copyright**

Other than for strictly personal use, it is not permitted to download, forward or distribute the text or part of it, without the consent of the author(s) and/or copyright holder(s), unless the work is under an open content license such as Creative Commons.

**Takedown policy**

Please contact us and provide details if you believe this document breaches copyrights.  
We will remove access to the work immediately and investigate your claim.

RESEARCH

Open Access



# Analytically estimating the efficiency of high temperature aquifer thermal energy storage

David Geerts<sup>1\*</sup>, Alexandros Daniilidis<sup>2</sup>, Gert Jan Kramer<sup>1</sup>, Martin Bloemendal<sup>2,3</sup> and Wen Liu<sup>1</sup>

Corresponding author at  
Copernicus Institute of  
Sustainable Development,  
Heidelberglaan 8, 3584 CS,  
Utrecht, The Netherlands.

\*Correspondence:  
d.c.geerts@uu.nl

<sup>1</sup> Copernicus Institute  
of Sustainable Development,  
Utrecht University, Princetonlaan  
8a, 3584 CB Utrecht, The  
Netherlands

<sup>2</sup> Faculty of Civil Engineering  
and Geosciences, Delft University  
of Technology, Stevinweg 1, 2628  
CN Delft, The Netherlands

<sup>3</sup> TNO - Geological Survey  
of the Netherlands, Princetonlaan  
6, 3584 CB Utrecht, The  
Netherlands

## Abstract

High-Temperature Aquifer Thermal Energy Storage (HT-ATES) can be used to reduce greenhouse gas emissions from heating. The thermal recovery efficiency is the main parameter indicating the performance of an HT-ATES system and it is influenced by multiple aquifer properties and storage characteristics. This study presents a method for estimating recovery efficiency through numerical modeling, data analysis, and curve fitting. This method shows the relation between the recovery efficiency and various storage conditions, such as aquifer properties and storage temperature. In addition, this research explores an analytical relationship between energetic efficiency and recovery efficiency and verifies that relationship with the generated data. The proposed method can be used for the purpose of initial screening to estimate the performance of an HT-ATES system and for efficiently using HT-ATES as a component in larger energy system models. This method uses the modified Rayleigh number in combination with aquifer thickness and injected volume and has a  $R^2$  of 85%. The analytical relation between energetic efficiency and recovery efficiency was shown to be accurate for all calculated energetic efficiency values above 60% and is less accurate with lower calculated energetic efficiency values.

**Keywords:** High-Temperature Aquifer Thermal Energy Storage (HT-ATES), Recovery efficiency, Energetic efficiency, Analytical approach

## Introduction

Greenhouse gas emissions mitigation, largely due to fossil fuel based energy use, is a major challenge in the twenty-first century. The heating and cooling of buildings accounts for approximately 65% of the global energy use in buildings IEA (2023), of which the majority is generated by fossil fuels Cozzi et al. (2020).

Aquifer Thermal Energy Storage (ATES) systems reduce greenhouse gas emissions by storing excess thermal energy and using it when there is a demand Hermans et al. (2018). This cycle can be repeated and is usually a seasonal cycle, storing heat during warm months and retrieving heat during cold months. This is graphically explained in Fig. 1.

In the Netherlands >3000 ATES systems have been installed. Most of these ATES systems store heat at a temperature of  $\leq 25$  °C Bloemendal and Hartog (2018). This temperature range is considered to be Low-Temperature Aquifer Thermal Energy

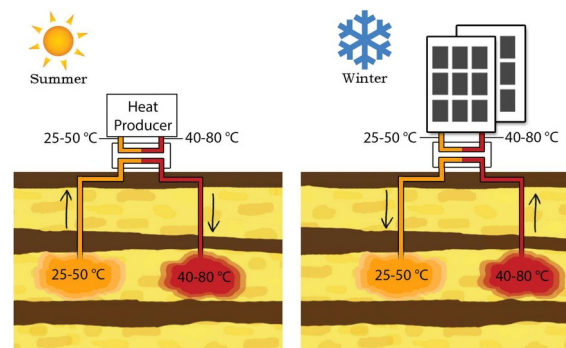


**Fig. 1** Operation modes of ATEs system, extracted from Bloemendal and Hartog (2018), left heating of the ATEs system, right cooling of the ATEs system, providing heat to buildings

Storage (LT-ATES). When higher temperatures are used, it is called HT-ATES. Which are typically described to have a temperature range between 50 and 90 °C Fleuchaus et al. (2020); Beernink et al. (2024); Heldt et al. (2024). ATEs systems operating Between a temperature of 25 and 50 °C are often called medium temperature ATEs Drijver et al. (2019). In this research HT-ATES refers to the entire range from 25 to 90 °C. Only a few HT-ATES systems are installed, most of them are experimental. Examples are described in Fleuchaus et al. (2020); Opel et al. (2017); van Loon and van der Heide (1992).

Using HT-ATES should in theory be beneficial as higher temperatures can be used in a wider range of applications, as well as direct use for most residential heating systems. Where the application of LT-ATES in space heating systems often needs a heat pump to increase the temperature Bloemendal and Hartog (2018) and is most efficient in newer, well-insulated buildings. HT-ATES, however, also suffer from practical drawbacks such as increased clogging, scaling and corrosion Sanner and Knoblich (1999); Holmslykke and Kjølner (2023). Higher injected temperature can also lead to more losses and, therefore, a lower Recovery Efficiency( $\eta_r$ ) Drijver et al. (2012); Beernink et al. (2024). This combined with the high upfront investment costs due to the drilling of wells, makes it important to accurately predict the  $\eta_r$  of an HT-ATES system in a specific subsurface location.

To calculate the  $\eta_r$ , simulation models are used which can compute the heat losses of an HT-ATES system. These models solve the groundwater flow and heat transfer equations using numerical methods and need expertise from professionals to build and correctly run them.

Previous studies have focused on optimizing ATEs systems Beernink et al. (2022); Duijff et al. (2023), yet methods for quickly estimating HT-ATES  $\eta_r$  remain limited. Rapid  $\eta_r$  estimation could facilitate the early identification of suitable sites. This paper presents a simple and computationally efficient approach to  $\eta_r$  estimation, offering a practical alternative to complex numerical models.

Previous research has developed similar tools to predict the  $\eta_r$ . An analytical approach was coined by Tang et al. Tang and Rijnaarts (2023) that showed how the  $\eta_r$  can be calculated analytically. Data-driven approaches have also been proposed. Where Schout et al. (2014) proposed a modified Rayleigh number, which was used to calculate the  $\eta_r$ . They specified injection temperatures between 55 °C and 90 °C and created 16 cases. Based on these cases an equation was created that used the modified Rayleigh number and

which captures the relation between the model input parameters and  $\eta_r$ . This temperature range was later extended to 90–300 °C by Sheldon et al. (2021). They focused on a larger amount of cases and proposed an equation for calculating  $\eta_r$  based on the same modified Rayleigh number. A recent study demonstrated that the  $\eta_r$  can be predicted based on the ratio between the Rayleigh number and Peclet number for convection-dominated regimes. For conduction-dominated regimes, the Peclet number, in combination with the volumetric heat capacity of the aquifer, was shown to correlate with the  $\eta_r$  Gao et al. (2024). All these studies showed a method for quickly determining the  $\eta_r$  of an ATES system.

This research extends the previous research done by Schout et al. Schout et al. (2014) as they used a limited number of input parameter values and likely missed interactions between parameters due to this. By extending the number and range of parameter values, new insights are gained into more subtle effects not encountered in the previous study. This study also differs from the research done by Sheldon et al. Sheldon et al. (2021). The used injection temperatures in this research are lower (25–80°C instead of 90–300°C), leading to less pronounced buoyancy flow. Furthermore, compared to their study, wider ranges of parameter values for some parameters are used. Compared to Gao et al. Gao et al. (2024) we use a larger number of parameters, where they only differed three parameters (aquifer permeability, flow rate and thermal conductivity of the cap rock), this work looks into the effects of seven different parameters. A refined version of the Rayleigh equation used by Schout et al. Schout et al. (2014) is proposed and analyzed. This equation is simple to use and transparent in how the efficiency is calculated, offering an alternative to the numerical models

In addition, this research introduces, explains, and analyzes the concept of Energetic Efficiency ( $\eta_e$ ) for an HT-ATES system. The  $\eta_e$  quantifies the useful energy delivered by the HT-ATES to a heating system, offering a more direct and practical measure of the efficiency of HT-ATES implementation. This metric is particularly significant for evaluating HT-ATES performance within heating systems because it assesses the actual portion of extracted heat that can be effectively utilized for heating purposes. In contrast, the  $\eta_r$  overlooks the interaction with the heating system, making the  $\eta_e$  a more applicable efficiency measure within heating systems. To the authors' knowledge, this parameter has not been explicitly discussed in prior literature. Only one study Daniilidis et al. (2022) has touched upon the  $\eta_e$ , exploring its impact on the techno-economic performance of an HT-ATES. In this work, we expand the knowledge by examining the relationship between  $\eta_r$  and  $\eta_e$  and presenting a formula to relate the two. To the authors' knowledge, this relationship, along with its validation, has not been previously published in the literature.

The objective of this paper is twofold. First, to develop a method for estimating the  $\eta_r$ , and second, to introduce, test, and analyze a relationship between  $\eta_r$  and  $\eta_e$ . Both objectives are achieved by running HT-ATES simulations using a Design of Experiments (DoE) approach over a broad yet representative range of subsurface and operational parameter values. This approach generates data on the variation in  $\eta_r$  and  $\eta_e$ . Using this data set, we evaluate the influence of each parameter on  $\eta_r$  and derive an equation based on the modified Rayleigh number, linking storage condition parameters to the expected  $\eta_r$  value. In addition, we test and validate the relationship between  $\eta_r$  and  $\eta_e$ , demonstrating its accuracy. These methods

enable the seamless integration of HT-ATES models into larger energy system models, thanks to their computational efficiency and simplicity.

## Method

### Definition $\eta_r$ and $\eta_e$

The  $\eta_r$  is defined as the ratio of extracted heat to injected heat compared to the ground temperature and this factor is very important for the feasibility of an HT-ATES system. The equation for  $\eta_r$  is adapted from Bloemendal et al. Bloemendal and Hartog (2018) assuming that the volume injected into the aquifer is the same as the volume extracted, which allows for unambiguous comparison of  $\eta_r$  values.

$$\eta_r = \frac{E_{out}}{E_{in}} = \frac{V_e \Delta T_e}{V_i \Delta T_i} = \frac{\overline{T_e} - T_g}{\overline{T_i} - T_g} \quad (1)$$

(see the nomenclature for the units used in the equations). The  $\eta_r$  shows the percentage of heat that is extracted compared to the injected heat. Note that in this study  $\eta_r$  only includes the subsurface losses, any other losses related to heat transport inside the wells or on the surface facilities are not included. The  $\eta_r$  changes over time, and generally increases during the first few years of operation until it stabilises. This research focuses on the stabilised  $\eta_r$  usually occurring after circa 8 years of operation.

An alternative approach to defining the efficiency of HT-ATES is by calculating the useful heat it delivers compared to the cutoff temperature. In district heating systems, heat is supplied to consumers at a certain temperature and returned at a lower temperature. The difference between the supply and return temperatures determines the amount of heat delivered. The return temperature, also known as the cutoff temperature, serves as the threshold, only temperatures above this threshold are considered useful for heating. Compared to the  $\eta_r$ , the  $\eta_e$  shows a direct measure of the efficiency within a heating system, where the  $\eta_r$  only shows the efficiency of the heating and cooling of the aquifer. The  $\eta_e$  is defined as:

$$\eta_e = \frac{E_{out}}{E_{in}} = \frac{V_e \Delta T_e}{V_i \Delta T_i} = \frac{V_e (\overline{T_e} - T_c)}{V_i (\overline{T_i} - T_c)} \quad (2)$$

This equation shows the percentage of useful heat extracted compared to the injected useful heat. Again this research focuses on the  $\eta_e$  of the eighth year, similar to the  $\eta_r$ . The relation between  $\eta_r$  and  $\eta_e$  is illustrated in Fig. 2. Assuming  $V_e = V_i$ , the  $\eta_r$  and  $\eta_e$  have the following relation:

$$\eta_e = \eta_r * \frac{T_i - T_g}{T_i - T_c} + \frac{T_g - T_c}{T_i - T_c}. \quad (3)$$

This equation is a simple analytical equation to quickly determine the  $\eta_e$ . However, the assumption that  $V_e = V_i$  is not always correct, as extraction ceases when the extracted temperature ( $T_e$ ) reaches the cutoff temperature ( $T_c$ ), which also suggests that Eq. 3 may not always be correct. To examine when the equation is correct and when it is not, we compare  $\eta_e$  values calculated via Eq. 3, called  $\eta_f$  ( $f$  stands for formula) with actual  $\eta_e$  values from the dataset, stopping extraction at  $T_e = T_c$ , called  $\eta_d$  ( $d$  stands for data).

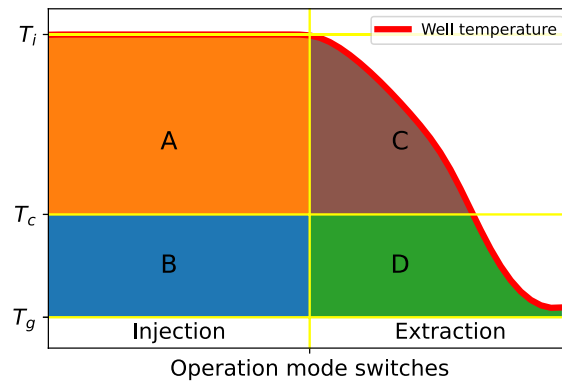


**Fig. 2** Temperature of hot HT-ATES well. The  $\eta_r = \frac{C+D}{A+B}$ , while the  $\eta_e = \frac{C}{A}$ .  $B$  is not used in the  $\eta_e$  equation, which implies that the cold well of the system has a 100% efficiency (both  $\eta_e$  and  $\eta_r$ ). This simplification is made as the primary focus of this research is focused on the hot well of the HT-ATES

Note that this calculation of  $\eta_d$  is an ex-post analysis after the model run as explained in "Model setup" section had been finished.  $\eta_d$  was calculated by using the extracted temperature profile from the model run. With this temperature profile the area  $C$  as defined in Fig. 2 is calculated and divided by the area  $A$  also defined in the same figure. Note that, in the MODFLOW model the well did not stop extracting when  $T_e = T_c$ ; therefore, the heat in the aquifer is depleted more than when extraction stops at  $T_e = T_c$ . This leads to decreased  $\eta_e$  values, compared to when extraction would stop at  $T_e = T_c$ .

Two cases are considered. Both cases have a different cutoff temperature, one cutoff temperature is defined as 20°C lower than the injected temperature ( $\Delta T_c = 20$ ) and the other as  $\Delta T_c = 30$ . These cases were chosen as HT-ATES is most feasible within a district heating grid and for these grids, the mentioned cutoff temperature differences are common Naber and Dehens (2022). Where smaller  $\Delta T_c$  are more common in district heating systems with low operating temperatures and larger  $\Delta T_c$  are more common in district heating systems with higher operating temperatures. For both cases, the  $\eta_e$  calculated using Eq. 3 is compared with the  $\eta_e$  calculated when the extraction stops when  $T_e = T_c$ , which is obtained from the data.

#### Important parameters for $\eta_r$

The value of  $\eta_r$  is dependent on the amount of recoverable heat from the subsurface and, therefore, dependent on heat losses to the subsurface. Heat losses can be attributed to heat conduction and heat convection, which will displace the heat so it can not be extracted Collignon et al. (2020). The conduction is proportional to the surface area-to-volume ratio Doughty et al. (1982), defined as:

$$\frac{A}{V_i} = \frac{2}{r_{th}} + \frac{2}{H}, \text{ where } r_{th} = \sqrt{\frac{c_w V_i}{c_{aq} \pi H}}, \quad (4)$$

here  $\eta_r$  increases when  $V_i$  increases. From this equation, it can be seen that important parameters for heat loss are likely the porosity, injected volume and thickness of the aquifer. Convection is shown to be dependent on horizontal and vertical hydraulic conductivity, aquifer thickness and injected fluid temperature Doughty et al. (1982);

Buscheck (1984); van Lopik et al. (2016). Conductive heat losses are dependent on the heat difference between the source and the surrounding, which in this case is the difference between the injected temperature and the ambient groundwater temperature. Therefore, the ambient groundwater temperature is also an important parameter.

The seven mentioned parameters and their effect on  $\eta_r$  are analysed in this research. A list of the parameters and the value range used for each parameter can be found in Table 4 with the respective references. This table is further explained in "Data generation" section. Anisotropy inside the aquifer is defined as

$$a = k_h/k_v \quad (5)$$

### Model setup

The model adopted by this research was developed in Bloemendal et al. Bloemendal and Hartog (2018). The software used is MODFLOW and SEAWATv4 coupled to a transport code MT3DMS. This model uses the finite difference method to solve the groundwater flow and heat transfer equations and has been used Bloemendal and Hartog (2018); Beernink et al. (2022); Todorov et al. (2020) and verified Visser et al. (2015); Mindel et al. (2021) in previous studies. To minimize run time an axisymmetric grid was used, which was shown to be able to correctly simulate an ATES system when there is radial symmetry, which is the case here Langevin (2008). With this approach, the results of the 2D model can be directly interpreted as equivalent to those of a 3D model, given the symmetry assumptions.

The model consists of 3 homogeneous layers, an aquifer layer of varying thickness, confined by two 30 m thick clay layers. All layers are set to have the ambient groundwater temperature at the beginning. The spatial discretization was 1 m in the vertical direction for the entire model domain. In the horizontal direction discretization was 1 m close to the well and from 200 to 2000 m away from the well, the cell size increased linearly until a cell size of 100 m is obtained at the boundary of the model, which is 2000 m away from the well. The boundaries are a constant head and constant temperature boundary, which also applies to the top and bottom edge of the model. A grid sensitivity was performed (see Sect. Appendix A) with varying grid cells size, until  $\eta_r$  varied less than 1% compared to smaller resolutions, this grid is visualized in Fig. 3. Any heat losses outside this aquifer domain are neglected in this study, e.g. transport losses.

One fully penetrating well is used that was located in the grid at  $x = 0$ . A typical HT-ATES system includes two wells; when spaced far enough apart, well interactions become negligible, allowing a single-well model to adequately capture the HT-ATES system's response. The well was assigned an injection and extraction pattern, which is a sinusoidal pattern, representing the seasonality of heat demand and supply. This pattern was 26 weeks of injecting followed by 26 weeks of extracting.

Temporal discretization of a week was used. The Courant condition is set to 0.8 in MT3DMS. MT3DMS automatically reduces time step to meet this condition, which is sufficiently small to capture important processes around the well Bloemendal and Hartog (2018); Duijff et al. (2023). The simulation period was eight years, after which the operation and  $\eta_r$  of the HT-ATES stabilized Beernink et al. (2024); Sheldon et al. (2021). Other parameters used in MODFLOW can be found in Table 1.



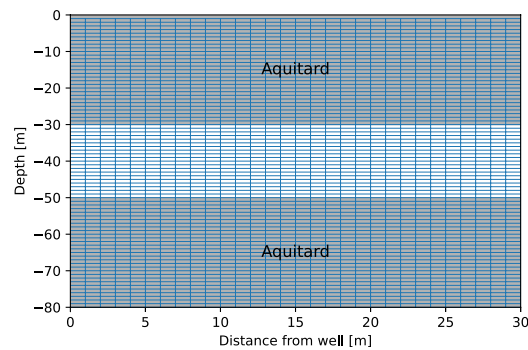


**Fig. 3** Example of grid discretization used for an aquifer thickness of 20 m, where the well is located at  $x = 0$ . Only the first 30 m are shown horizontally, this discretization is used until 200 m away from the well

**Table 1** Parameters used in the simulations

Parameter	Value	Unit
Density solids	2640	$\text{kg m}^{-3}$
Specific heat capacity solids	710	$\text{J kg}^{-1} \text{K}^{-1}$
Specific heat capacity fluids	4183	$\text{J kg}^{-1} \text{K}^{-1}$
Well radius	0.3	m
Aquitards horizontal permeability	0.05	$\text{m day}^{-1}$
Aquitards vertical permeability	0.01	$\text{m day}^{-1}$

### Model verification

The created model was verified with previously published results. Multiple studies have used MODFLOW to simulate an ATEs system and have proven that the simulator is accurate for such models Visser et al. (2015); Bonte et al. (2013); van der Roest et al. (2021); Bloemendal and Hartog (2018). They also pointed out that real cases are often more complicated than the simulation and discrepancies between the software and reality exist due to this complexity.

MODFLOW/SEAWAT and MT3DMS are shown to be comparable in capabilities and results with MOOSE, MARTHE and Nexus-CSMP++ Mindel et al. (2021). The model used in this research is nonetheless compared with earlier research from Sheldon et al. (2021) to check whether the results of the model in terms of  $\eta_r$  are in line with their results. While exact alignment between models is not expected due to potential differences in simulation setups (such as solver conditions or grid discretization), significant discrepancies would suggest potential modeling errors. This verification step helps identify any inconsistencies.

Eight scenarios were created to facilitate the comparison. These scenarios are based on the values of  $V_i$ ,  $H$ ,  $k_h$  and  $a$  as was done in Sheldon et al. (2021). The values used in the scenarios can be found in Table 2. The scenarios exclude changes in  $T_i$ , because the lowest value used in Sheldon et al. (2021) was already higher than the highest value in this research, and therefore, this lowest value was chosen, which was  $90^\circ\text{C}$ . Values for  $T_g$  and  $n$  were set in line with Sheldon et al. Sheldon et al. (2021) and shown in Table 3.



**Table 2** Scenarios for comparing the models

Name	$V_i$	$H$	$k_h$	$\alpha$
Base	1E5	60	1	10
$V^l$	5E4	60	1	10
$V^h$	2E5	60	1	10
$k^h$	1E5	60	10	10
$H^l$	1E5	20	1	10
$\alpha^h$	1E5	60	1	100
$V^l k^h H^l$	5E4	20	10	10
$V^h k^h \alpha^h H^l$	2E5	20	10	100

The name refers to the parameters that are changed compared to the base case. The superscript refers to the direction of the change: heightened (*h*) or lowered (*l*)

### Data generation

The data were generated running simulations as described in "Model setup" section and consisted of two parts. The first part is a full factorial design, according to the DoE theory Antony (2023). This design has the advantage that the complete parameter space is explored and every possible combination of values listed in Table 4 was modeled and the corresponding  $\eta_r$  was calculated. The DoE design was supplemented by using the mean values of all input parameters. These mean values were also combined with all possible other values. Two exceptions that did not use the mean were (1) ground temperature, which is expected to only influence  $\eta_r$  based on the difference with injected temperature (see "Important parameters for  $\eta_r$ " section). (2) For injected volume, the logarithmic mean was used due to the fact that the diameter of the thermal plume of the warm well increases logarithmically and losses are shown to be dependent on the size of the thermal plume Bloemendal and Hartog (2018).

**Table 3** Parameters used in model verification that are different between "Model setup", "Data generation" and "Model verification" sections

Parameter	Value	Unit
Porosity	0.25	–
Ground temperature	28	°C

**Table 4** Parameter ranges for simulations using a full factorial DoE. A total of 3418 forward simulations were run, of which 1458 with the DoE design and 1960 with the random design

Parameter	Used values	Unit	Source
Porosity	0.1, 0.2, 0.3	–	Cherry and Freeze (1979)
Injected volume	$10^4$ , $10^5$ , $10^6$	m <sup>3</sup>	Bloemendal and Hartog (2018)
Injected temperature	25, 52.5, 80	°C	Bloemendal and Hartog (2018); Birdsell et al. (2021) <sup>a</sup>
Ambient ground temperature	10, 30	°C	Bloemendal and Hartog (2018); Rijksoverheid (2023) <sup>b</sup>
Horizontal hydraulic conductivity	1, 43, 85	m day <sup>-1</sup>	Sheldon et al. (2021); Cherry and Freeze (1979)
Anisotropy (see Eq. 5)	1, 50, 100	–	Cherry and Freeze (1979)
Aquifer thickness	20, 62, 105	m	Bloemendal and Hartog (2018)

<sup>a</sup> Definition temperature range of LT and HT-ATES

<sup>b</sup> Common temperature at depths <500 m (depth that is outside of dutch mining regulation)

The second part of the data generation was based on a completely randomized design, where each parameter was randomized between its minimum and maximum value. This was done to better capture any non-linearity in the relationship between the inputs and the  $\eta_r$  values. 1458 forward simulations were run using the DoE design and 1960 forward simulations were run using the randomized design.

As the focus of this research is the  $\eta_r$  value of the hot well, the data points corresponding to a smaller injection temperature than the ambient ground temperature were removed. One example is the combination of an injected temperature of 25 °C and an ambient ground temperature of 30 °C (shown in Table 4).

### $\eta_r$ determination

First, a Distant-based Global Sensitivity Analysis (DGSA) Fenwick et al. (2014) was performed to determine whether the variation in each individual parameter significantly affects the  $\eta_r$  value. For this analysis, the data was divided into three clusters: one containing high  $\eta_r$  values, one with average  $\eta_r$  values, and one with low  $\eta_r$  values. This clustering was achieved by solving the k-medoids problem Fenwick et al. (2014). The parameter values associated with the three clusters were then compared to parameter values obtained through random sampling of the dataset, with the sampled clusters matching the size of the original three clusters. A parameter was considered significant if the difference in parameter values between the two clusters of the same size exceeded 1. Essentially showing whether changing a certain parameter, significantly changes the  $\eta_r$ . This DGSA analysis was used to identify parameters that do not significantly contribute to the variability in  $\eta_r$ , allowing them to be excluded from further analysis. This analysis was carried out using the pyDGSA package, using 3 clusters and 3000 boots Perzan et al. (2021).

Second, the  $\eta_r$  value was estimated by creating an equation which equates the relevant parameters with the  $\eta_r$  value. This equation is simple to use compared to other methods that estimate a single number, such as machine learning. The modified Rayleigh number ( $Ra^*$ ) was used as proposed by Schout et al. (2014), who used the following formula:

$$\eta_r = Ae^{BRa^*}. \quad (6)$$

Where  $A$  and  $B$  were originally functions of aquifer thickness and  $Ra^*$  is obtained from Schout et al. (2014) and is

$$Ra^* = \frac{\alpha_f \bar{\rho} g H^2 c_a \sqrt{k_h k_v} \Delta T}{\bar{\mu} \lambda_a R_{th}}. \quad (7)$$

Both  $\bar{\rho}$  and  $\bar{\mu}$  are evaluated at the average water temperature defined as  $(T_i + T_g)/2$ . This research extends the curve fitting done in Schout et al. (2014) by using a wider range of operating and subsurface conditions. A new curve is fitted using the Levenberg–Marquardt algorithm Ranganathan (2004), as implemented in the scipy.optimize library Virtanen et al. (2020).

## Results

### Model verification and comparison of results between one and two-wells model

The results of the eight scenarios are shown in Fig. 4. As can be seen 7 of the 8 scenarios differ by a maximum of 1%. Only one scenario differs by 2%. The observed differences can be caused by simulator setup differences and grid discretization, for example, Sheldon et al. Sheldon et al. (2021) used a triangular grid structure that could not be replicated. Nonetheless, both simulators exhibit consistent trends in  $\eta_r$  with changing parameters, indicating similar parameter interactions and confirming comparable outcomes across both simulators. When the models would be set up exactly the same, the results would align even better Mindel et al. (2021); however, this was not the objective of this verification.

### Factorial design results

Table 5 presents the data created with the full factorial design. The table shows the  $\eta_r$  value for each of the used parameter values. This table can be used to look up  $\eta_r$  when the values of the parameters are close to the used values in the simulations.  $\eta_r$  values range from 1% to 92%, with 70% of data points being larger than 50% and 33% being larger than 80%. A general trend is that the  $\eta_r$  value is higher with higher injected volume, which is in line with previous research Beernink et al. (2019). Another observation is that low anisotropy coupled with high  $k_h$  values leads to a low  $\eta_r$ , due to increased buoyancy flow. This effect is most prominent with high aquifer thickness due to the increased space for buoyancy flow to manifest. The highest  $\eta_r$  values are observed at large thickness with large injected volume and low horizontal hydraulic conductivity (having  $\eta_r$  values between 88%-92%).

Compared to the randomized data points, the  $\eta_r$  values of the DoE design are more extreme. For example the smallest  $\eta_r$  achieved with the randomized data points is 20%, compared to 1% of the DoE data points. The randomized data points also have a higher average  $\eta_r$  which was 82% compared to 68% for the DoE data points.

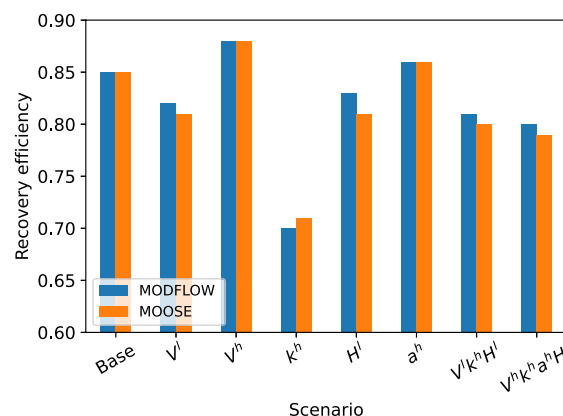


**Fig. 4** Comparison with Sheldon et al. Sheldon et al. (2021).  $\eta_r$  values were rounded to two significant numbers

**Table 5**  $\eta_r$  (in %) at year eight of the simulation for each design of experiment data point

			$H$	20									62									105																																																																																																																																																																																																																																																																																																																																																																																																																																																																																																																										
				1			43			85			1			43			85			1			43			85																																																																																																																																																																																																																																																																																																																																																																																																																																																																																																																				
				$k_h$	$a$	$n$	$T_i$	$T_g$	$V_i$	$n$	$T_i$	$T_g$	$V_i$	$n$	$T_i$	$T_g$	$V_i$	$n$	$T_i$	$T_g$	$V_i$	$n$	$T_i$	$T_g$	$V_i$	$n$	$T_i$	$T_g$	$V_i$	$n$	$T_i$	$T_g$	$V_i$	$n$	$T_i$	$T_g$	$V_i$	$n$	$T_i$	$T_g$	$V_i$	$n$	$T_i$	$T_g$	$V_i$	$n$	$T_i$	$T_g$	$V_i$	$n$	$T_i$	$T_g$	$V_i$	$n$	$T_i$	$T_g$	$V_i$	$n$	$T_i$	$T_g$	$V_i$	$n$	$T_i$	$T_g$	$V_i$	$n$	$T_i$	$T_g$	$V_i$	$n$	$T_i$	$T_g$	$V_i$	$n$	$T_i$	$T_g$	$V_i$	$n$	$T_i$	$T_g$	$V_i$	$n$	$T_i$	$T_g$	$V_i$	$n$	$T_i$	$T_g$	$V_i$	$n$	$T_i$	$T_g$	$V_i$	$n$	$T_i$	$T_g$	$V_i$	$n$	$T_i$	$T_g$	$V_i$	$n$	$T_i$	$T_g$	$V_i$	$n$	$T_i$	$T_g$	$V_i$	$n$	$T_i$	$T_g$	$V_i$	$n$	$T_i$	$T_g$	$V_i$	$n$	$T_i$	$T_g$	$V_i$	$n$	$T_i$	$T_g$	$V_i$	$n$	$T_i$	$T_g$	$V_i$	$n$	$T_i$	$T_g$	$V_i$	$n$	$T_i$	$T_g$	$V_i$	$n$	$T_i$	$T_g$	$V_i$	$n$	$T_i$	$T_g$	$V_i$	$n$	$T_i$	$T_g$	$V_i$	$n$	$T_i$	$T_g$	$V_i$	$n$	$T_i$	$T_g$	$V_i$	$n$	$T_i$	$T_g$	$V_i$	$n$	$T_i$	$T_g$	$V_i$	$n$	$T_i$	$T_g$	$V_i$	$n$	$T_i$	$T_g$	$V_i$	$n$	$T_i$	$T_g$	$V_i$	$n$	$T_i$	$T_g$	$V_i$	$n$	$T_i$	$T_g$	$V_i$	$n$	$T_i$	$T_g$	$V_i$	$n$	$T_i$	$T_g$	$V_i$	$n$	$T_i$	$T_g$	$V_i$	$n$	$T_i$	$T_g$	$V_i$	$n$	$T_i$	$T_g$	$V_i$	$n$	$T_i$	$T_g$	$V_i$	$n$	$T_i$	$T_g$	$V_i$	$n$	$T_i$	$T_g$	$V_i$	$n$	$T_i$	$T_g$	$V_i$	$n$	$T_i$	$T_g$	$V_i$	$n$	$T_i$	$T_g$	$V_i$	$n$	$T_i$	$T_g$	$V_i$	$n$	$T_i$	$T_g$	$V_i$	$n$	$T_i$	$T_g$	$V_i$	$n$	$T_i$	$T_g$	$V_i$	$n$	$T_i$	$T_g$	$V_i$	$n$	$T_i$	$T_g$	$V_i$	$n$	$T_i$	$T_g$	$V_i$	$n$	$T_i$	$T_g$	$V_i$	$n$	$T_i$	$T_g$	$V_i$	$n$	$T_i$	$T_g$	$V_i$	$n$	$T_i$	$T_g$	$V_i$	$n$	$T_i$	$T_g$	$V_i$	$n$	$T_i$	$T_g$	$V_i$	$n$	$T_i$	$T_g$	$V_i$	$n$	$T_i$	$T_g$	$V_i$	$n$	$T_i$	$T_g$	$V_i$	$n$	$T_i$	$T_g$	$V_i$	$n$	$T_i$	$T_g$	$V_i$	$n$	$T_i$	$T_g$	$V_i$	$n$	$T_i$	$T_g$	$V_i$	$n$	$T_i$	$T_g$	$V_i$	$n$	$T_i$	$T_g$	$V_i$	$n$	$T_i$	$T_g$	$V_i$	$n$	$T_i$	$T_g$	$V_i$	$n$	$T_i$	$T_g$	$V_i$	$n$	$T_i$	$T_g$	$V_i$	$n$	$T_i$	$T_g$	$V_i$	$n$	$T_i$	$T_g$	$V_i$	$n$	$T_i$	$T_g$	$V_i$	$n$	$T_i$	$T_g$	$V_i$	$n$	$T_i$	$T_g$	$V_i$	$n$	$T_i$	$T_g$	$V_i$	$n$	$T_i$	$T_g$	$V_i$	$n$	$T_i$	$T_g$	$V_i$	$n$	$T_i$	$T_g$	$V_i$	$n$	$T_i$	$T_g$	$V_i$	$n$	$T_i$	$T_g$	$V_i$	$n$	$T_i$	$T_g$	$V_i$	$n$	$T_i$	$T_g$	$V_i$	$n$	$T_i$	$T_g$	$V_i$	$n$	$T_i$	$T_g$	$V_i$	$n$	$T_i$	$T_g$	$V_i$	$n$	$T_i$	$T_g$	$V_i$	$n$	$T_i$	$T_g$	$V_i$	$n$	$T_i$	$T_g$	$V_i$	$n$	$T_i$	$T_g$	$V_i$	$n$	$T_i$	$T_g$	$V_i$	$n$	$T_i$	$T_g$	$V_i$	$n$	$T_i$	$T_g$	$V_i$	$n$	$T_i$	$T_g$	$V_i$	$n$	$T_i$	$T_g$	$V_i$	$n$	$T_i$	$T_g$	$V_i$	$n$	$T_i$	$T_g$	$V_i$	$n$	$T_i$	$T_g$	$V_i$	$n$	$T_i$	$T_g$	$V_i$	$n$	$T_i$	$T_g$	$V_i$	$n$	$T_i$	$T_g$	$V_i$	$n$	$T_i$	$T_g$	$V_i$	$n$	$T_i$	$T_g$	$V_i$	$n$	$T_i$	$T_g$	$V_i$	$n$	$T_i$	$T_g$	$V_i$	$n$	$T_i$	$T_g$	$V_i$	$n$	$T_i$	$T_g$	$V_i$	$n$	$T_i$	$T_g$	$V_i$	$n$	$T_i$	$T_g$	$V_i$	$n$	$T_i$	$T_g$	$V_i$	$n$	$T_i$	$T_g$	$V_i$	$n$	$T_i$	$T_g$	$V_i$	$n$	$T_i$	$T_g$	$V_i$	$n$	$T_i$	$T_g$	$V_i$	$n$	$T_i$	$T_g$	$V_i$	$n$	$T_i$	$T_g$	$V_i$	$n$	$T_i$	$T_g$	$V_i$	$n$	$T_i$	$T_g$	$V_i$	$n$	$T_i$	$T_g$

The green color refers to higher  $\eta_r$  values, where the red color refers to lower  $\eta_r$  values

### Distant-based global sensitivity analysis

The DGSA shows that all of the sensitivity indices are significantly larger than one, which supports the statement that all of these parameters do influence the variance in  $\eta_r$  (Fig. 5). None of the parameters can be excluded based on the DGSA. What can also be seen is that four parameters should be able to explain large part of the variance in  $\eta_r$ , namely injected volume, injected temperature, anisotropy and horizontal hydraulic conductivity. In contrast the three remaining parameters might not be able to explain a lot of variance, which are ground temperature, porosity and aquifer thickness.

### Curve fitting

A formula was fitted to the data (see Eq. 6). In Schout et al. Schout et al. (2014) the  $A$  and  $B$  terms were functions of aquifer thickness. To check the validity of only using

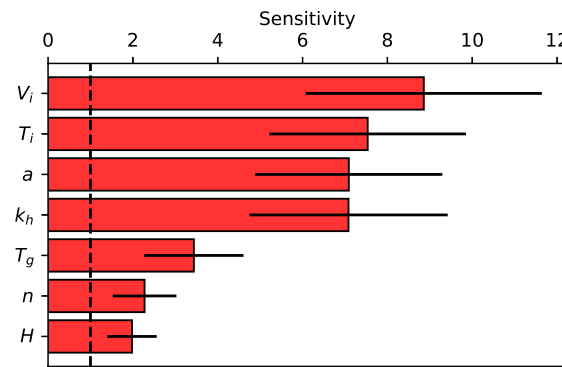


**Fig. 5** Results of the DGSA with their uncertainty. A value below 1 means that the parameters does not significantly impact the  $\eta_r$

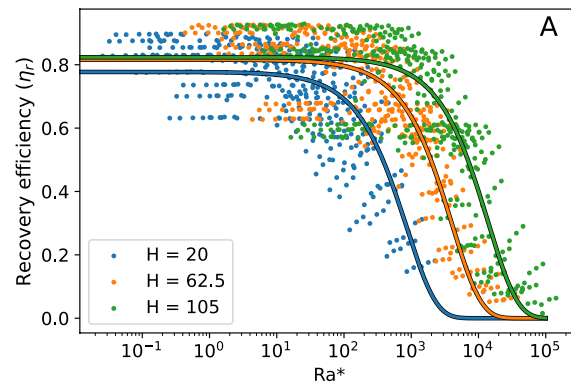
aquifer thickness, the A and B terms were tested as a function of every individual parameter. Of all parameters, only the aquifer thickness and injected volume significantly increased the  $R^2$  compared to when A and B are single numbers and not functions of any parameter. In the case of A and B being individual numbers, the  $R^2$  is 0.55 and A and B term values are 0.77 and  $-1.0e-4$  respectively. The resulting fitting for thickness and volume can be found in Fig. 6a and b respectively. Both individual parameters have a relatively low  $R^2$  compared to Schout et al. Schout et al. (2014) who found an average  $R^2$  of 94%. Therefore, injected volume and aquifer thickness are combined in one formula, which increases  $R^2$  to 0.85 and coefficients are as follows:

$$\eta_r = \left(0.406 - \frac{2.02e3}{V}\right) e^{Ra^* \left(\frac{2.46}{V} - 2.62e-4\right)} + \left(0.500 - \frac{1.37}{V}\right) e^{Ra^* \left(\frac{-3.92e-2}{V} - 3.25e-4\right)} \quad (8)$$

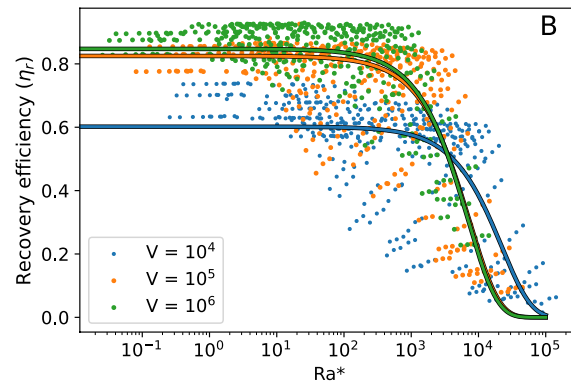
The fitting of this formula is shown in Fig. 6c. As observed, including both the injected volume and aquifer thickness enhances the formula's accuracy. This result appears to contrast with the findings of the DGSA, where aquifer thickness has the lowest sensitivity index. However, it is important to note that the DGSA provides a general analysis and using the modified Rayleigh number is a specific approach to predicting  $\eta_r$ . When using the modified Rayleigh number, a significant portion of the correlation between input parameters and  $\eta_r$  is already accounted for. The only effects not fully captured by the modified Rayleigh number are those of the injected volume and aquifer thickness.

The  $R^2$  in this study is 9 percentage points lower than that found by Schout et al. Schout et al. (2014) (from on average 94–85%), which can be attributed to the broader parameter range and larger dataset used here. This expanded range captures more complex interactions between parameters, indicating that the formula is accurate only within the narrower parameter limits they selected.

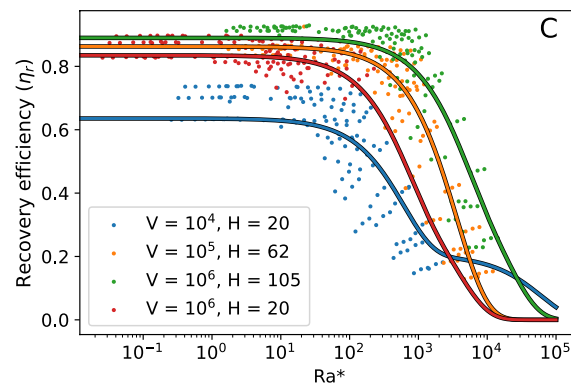
Compared to Sheldon et al. Sheldon et al. (2021) the  $R^2$  in this study is lower by 3 percentage point (from 88 to 85%). However, they only use aquifer thickness in their formula. This difference is due to the chosen range in aquifer thickness. The smaller aquifer thicknesses used in their work, were shown to be completely explained by the  $Ra^*$  coupled to the thickness leading to a very high  $R^2$ . These aquifer thicknesses



(a) A fitted curve with  $Ra^*$  and aquifer thickness included, where  $A = 0.836 + \frac{-1.16}{H}$  and  $B = \frac{-2.71e-2}{H} + 1.86e-4$ .  $R^2$  of the fitted formula is 0.73.



(b) A fitted curve with  $Ra^*$  and yearly injected volume included, where  $A = 0.85 + \frac{-2.48e3}{V}$  and  $B = \frac{1.01}{V} - 1.46e-4$ .  $R^2$  of the fitted formula is 0.65.

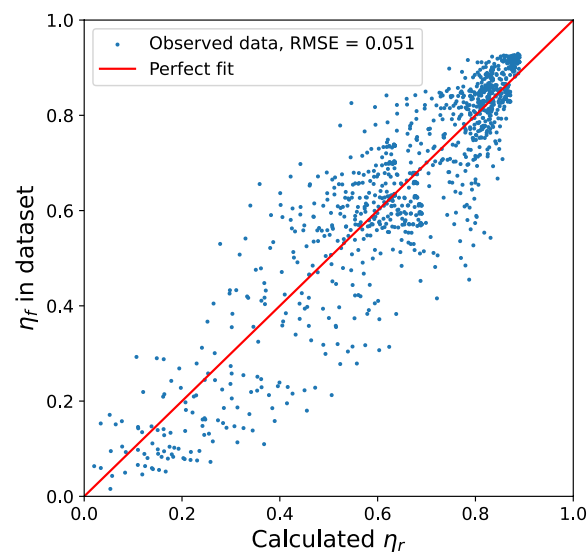


(c) A fitted curve with  $Ra^*$ , yearly injected volume and aquifer thickness included, see Eq. 8.  $R^2$  of the fitted formula is 0.85. Only a selection of volume and thickness combinations is shown for readability.

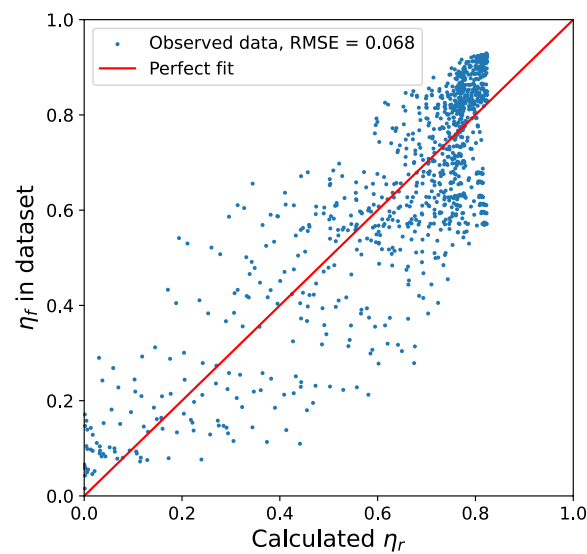
**Fig. 6** Results of curve fitting

were not included in this research leading to a lower  $R^2$  and the need to also include injected volume in the fitted formula. Furthermore a wider range of injected volume was used in this study. Which might increase the effect that injected volume has on  $\eta_r$ .

The predictive capacity of the formula was also tested using the RootMean Square Error (RMSE) Hodson (2022). With Eq. 8, the RMSE is reduced by 1.7 percentage points compared to only using the thickness in the fitting formula (Fig. 7). When thickness alone is used, the formula imposes a limit on  $\eta_r$  at 0.836 (Fig. 7b), while many data points exceed this value, reducing accuracy for higher  $\eta_r$  values. However, Eq. 8 resolves this problem, improving accuracy at higher  $\eta_r$  values. This shows that



(a) Error in the prediction using Eq. 8.



(b) Error in the prediction using  $A$  and  $B$  described in Fig. 6a.

**Fig. 7** Error in the different curve fitting



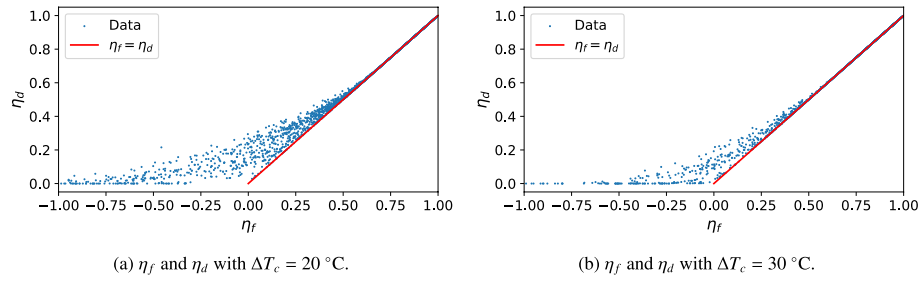


**Fig. 8**  $\eta_f$  and  $\eta_d$  values for the data points considering different cutoff temperatures. Negative values occur of  $\eta_f$  occur when  $T_e$  is smaller than  $T_c$  in Eq. 2

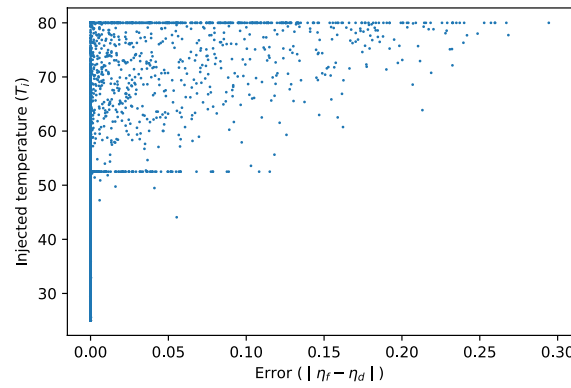


**Fig. 9** Error of the formula plotted against the injected temperature with  $\Delta T_c = 20$ , the increased number of data points at  $T_i = 80$  & 52 are due to the DoE design using only these values

incorporating injected volume into the formula enhances for both  $R^2$  and RMSE and is important for calculating the  $\eta_r$ .

#### Difference $\eta_r$ and $\eta_e$

Equation 3 can be used to calculate  $\eta_e$  from  $\eta_r$ . This part of the results explores when the equation is accurate and when it is not.

As shown in Fig. 8a, with  $\Delta T_c = 20$  °C (Reminder,  $\Delta T_c = T_i - T_c$ ), Eq. 3 is more accurate for higher  $\eta_f$  values. Specifically, when  $\eta_f \geq 0.6$ , the estimation error is less than 1% and the error tends to increase as  $\eta_f$  decreases. Where error is defined as  $|\eta_f - \eta_d|$  and all values of  $\eta_f$  below zero are set to zero. This increasing error is because with a lower estimated  $\eta_f$  the chance that the extracted temperature reaches the cutoff temperature is larger. When that happens the assumption that  $V_e = V_i$  is not valid and  $\eta_f$  starts to differ from  $\eta_d$ . This is more often the case at low  $\eta_f$  values, but not always and some points with low  $\eta_f$  have a error below 1 percentage point.

The injected temperature correlates most strongly with the error in  $\eta_f$ , while the other input parameters correlate only weakly with the error in  $\eta_f$  (Fig. 9). With larger injected temperature the errors increase on average, but even at an injected temperature of 80 °C 33% of data points have an error below 1 percentage point and 62% have an error below 5%. However, as mentioned, district heating systems operating at higher temperatures typically operate at a larger  $\Delta T_c$  Naber and Dehens (2022). The cutoff temperature significantly influences the accuracy of Eq. 3 (Fig. 8). When the cutoff temperature

decreases,  $\Delta T_c$  increases, increasing the likelihood that  $V_i = V_e$  since the probability of  $T_c \geq T_e$  increases with a larger  $\Delta T_c$ .

When the  $\Delta T_c$  is 30 the differences between  $\eta_f$  and  $\eta_d$  becomes smaller and Eq. 3 is more accurate (Fig. 8b). The error is smaller than 1% for all  $\eta_f$  values above 0.5. HT-ATES systems with a  $\eta_e$  below 50% are likely less economically attractive.

## Discussion

This research shows a method for quickly determining the  $\eta_r$  of an HT-ATES system. Furthermore it shows an analytical relation between the  $\eta_r$  and  $\eta_e$  and tests the accuracy of the relationship. This allows for quick identification of suitable locations for HT-ATES by first determining the  $\eta_r$  using Eq. 8 and then converting this  $\eta_r$  to the  $\eta_e$ , which shows the potential contribution of HT-ATES to a heating system. This method also facilitates integration of HT-ATES systems into larger energy system simulations without the computational burden of a detailed physics-based model.

This research also identified and tested an analytical relationship between  $\eta_r$  and  $\eta_e$  (Eq. 3) and found that this relationship is most accurate for high calculated  $\eta_e$  values. However, several factors may affect this accuracy. First, the model assumes 100% efficiency for the cold well, which is unrealistic; in practice, the cold well's  $\eta_r$  would likely resemble that of the hot well, leading to a lower calculated  $\eta_e$ . Second, the model assumes a fixed cutoff temperature, though in reality, this threshold can vary with external conditions. In addition, cutoff temperatures are dependent on insulation among other factors. These factors are subject to change, increasing or decreasing the cutoff temperature, and therefore, the  $\eta_e$  of the HT-ATES. Lastly, the  $\eta_e$  is calculated for data points that keep a volume balance at all times. In practice, when  $T_e = T_c$ , extraction would stop, leaving more heat in the subsurface, possibly increasing the  $\eta_e$  in subsequent years. Preliminary test suggest that this effect is minor (<2%), but future research can explore this further.

This method also has limits as the prediction of  $\eta_r$  can not explain all the variability in the  $\eta_r$ . Other methods are possible that can predict the  $\eta_r$ , examples are machine learning Sheldon et al. (2021); Geerts et al. (2025), or linear interpolation from the data in Table 5. These methods are likely to be more accurate Zielesny (2011); however, they lack the insight that the formula in Eq. 8 offers, which showed that volume and thickness coupled to the modified Rayleigh number are the most important parameters affecting the  $\eta_r$ . This formulation shows analytically what parameters should change and how to increase the  $\eta_r$ . The proposed method was chosen due to its transparency of calculation method and simplicity, which comes at the cost of accuracy. Another approach would be to use the Peclet number, which was proposed in Gao et al. (2024) and would be an alternative approach for future research. Another limitation is that the equation still requires detailed information on the subsurface, which has to be measured or estimated before this equation can be used.

To make a feasibility assessment for an HT-ATES installation, there are other considerations that need to be taken into account to be able to use the results of this research appropriately. These considerations can be divided into four types:

1. Other subsurface conditions not studied in this work might need investigation. First, other nearby wells or boreholes can positively or negatively affect the  $\eta_r$  of the HT-

ATES system, e.g. nearby ATES systems or BTES systems. In Duijff et al. Duijff et al. (2023) it was determined that the mutual interaction effect of ATES can be minimized by placing them far apart. However, this spacing is often not possible due to practical constraints such as the piping and other underground activities Çomaklı et al. (2004). Consequently the HT-ATES wells are placed closer together and they might interact with each other, influencing the  $\eta_r$ . Second, is the ambient groundwater flow, that can affect the  $\eta_r$ . Bloemendal et al. Bloemendal and Hartog (2018) showed that change in  $\eta_r$  related to ambient groundwater flow in the aquifer can be written in relation to  $r_{th}/u$ . They also showed that when groundwater flow is higher, the ratio  $\frac{L}{r_{th}}$  should be below 1, where  $L$  is the injection screen length. Another study showed that the ambient groundwater flow can be advantageous if well design is adapted, which was coined to be a unidirectional ATES Silvestri et al. (2025). Lastly, the aquifer was assumed to be homogeneous, despite the expectation of heterogeneity in real-world aquifers Visser et al. (2015). Aquifer heterogeneity is highly site-specific, and its effect on the  $\eta_r$  depends on the type and extent of heterogeneity present. Previous studies have shown that heterogeneity influences both the  $\eta_r$  and the thermal distribution of the hot plume Visser et al. (2015); Sommer et al. (2013). The impact of heterogeneity on  $\eta_r$  can vary significantly; for instance, Visser et al. Visser et al. (2015) reported a reduction in  $\eta_r$  due to heterogeneity in their specific case study. However, due to the site-specific nature of these effects, heterogeneity was not considered in this work.

2. System-level considerations such as the availability of heat demand and proximity to heat transport infrastructure is crucial to be able to use the stored heat efficiently and minimize transport losses, which were found to be between 5-35% and should be taken into account Werner (2017).
3. Regulations have to be taken into account in the decision-making. Examples are that some areas or aquifers are protected due to drinking water extraction Stemmler et al. (2022) or restrictive use of the subsurface area Bloemendal et al. (2018).
4. Lastly the economic feasibility of the HT-ATES system depends on factors such as price of heat used for charging and the price of the stored heat, cost of drilling, the optional installation of an heat pump and possible subsidy schemes for HT-ATES Daniilidis et al. (2022). Previous research has shown that  $\eta_r$  alone is not a sufficient predictor for good economic performance Daniilidis et al. (2022); Beernink et al. (2022) and that a minimum transmissivity and system capacity is required to make HT-ATES competitive with other storage options Daniilidis et al. (2022).

All these consideration are important for the successful installation and operation of an HT-ATES system.

## Conclusion

In this research a method was developed to estimate the  $\eta_r$  value of an HT-ATES system for temperatures in the range of 25-80 °C. First, a numerical model was built to represent the subsurface part of an HT-ATES system. The model was validated with Sheldon et al. (2021) and the models show comparable  $\eta_r$  values.

The model was then run repeatedly for a wide range of relevant subsurface and design parameters to generate data on the relationship between these input parameters and the  $\eta_r$  values. Based on this data, an equation was fitted to the data using the modified Rayleigh number. This equation achieved an  $R^2$  of 85% and offers robust predictive capability for  $\eta_r$  within the tested parameter range (Eq. 8). In addition, Table 5 was presented from which the  $\eta_r$  can be read when the parameters are known. This table has the exact simulation outcomes. Both the equation and the table can be used to identify suitable HT-ATES sites, after which more detailed modelling might still be necessary depending on the location's unique situation.

An analytical relation between the  $\eta_e$  and  $\eta_r$  was developed and tested (Eq. 3). It was shown that the used relation is accurate for those data points where the calculated  $\eta_e$  is larger than 50% when the difference between injected temperature and cutoff temperature is 30°C. Using a difference of 20°C this threshold is 60%. Below these thresholds, the  $\eta_e$  estimate may be less precise but can still offer a useful indication for feasibility assessment. HT-ATES systems with  $\eta_e$  values below this threshold are likely not feasible from an economic perspective and further investigation for these cases would be needed.

With this research first the  $\eta_r$  can be estimated using the proposed formula (Eq. 8) after which the  $\eta_e$  can be calculated using Eq. 3. Coupling these two equations shows the efficiency of an HT-ATES within an heating system. By coupling the two equations, suitable HT-ATES sites can be quickly identified and the usefulness of the HT-ATES within a heating system can be calculated.

## Appendix

### Grid sensitivity

This section presents the grid sensitivity analysis performed to evaluate the impact of grid block size on the calculated  $\eta_r$ . For 10 randomly selected points in the DoE design the difference in  $\eta_r$  was calculated between different grid block sizes. The following grid block sizes were used:

1. 0.25 x 0.25 (x-direction x z-direction) m blocks
2. 0.5 x 0.5 m blocks
3. 1 x 0.5 m blocks
4. 0.5 x 1 m blocks
5. 1 x 1 m blocks
6. 2 x 2 m blocks

The baseline simulation was conducted using 0.25 x 0.25 m grid blocks, and all other grid sizes were compared to this baseline. The relative difference,  $\sigma$ , was calculated using the following equation:

$$\sigma = \eta_r - \eta_{r,base} \quad (9)$$

where  $\eta_{r,base}$  is the  $\eta_r$  of the simulation using grid blocks of 0.25 x 0.25 m.

**Table 6** Average and maximum  $\sigma$  values obtained from the grid sensitivity analysis for the 10 data points tested

Block size	Average $\sigma$ (%)	Highest $\sigma$ (%)
0.5 x 0.5m	0.02	0.08
0.5 x 1m	0.07	0.20
1 x 0.5m	0.08	0.18
1 x 1m	0.15	0.35
2 x 2m	1.1	3.2

Table 6 shows the resulting  $\sigma$ . The 1 x 1 m has both the average and maximum  $\sigma$  below 1%, while for the 2 x 2 m blocks both the average and maximum  $\sigma$  are above 1%. Therefore, the 1 x 1 blocks were used.

#### Abbreviations

$\alpha_f$	Coefficient of thermal expansion of water $K^{-1}$
$\Delta T$	Difference between injected and ground temperature $^{\circ}C$
$\eta_e$	Energetic efficiency -
$\eta_I$	Energetic efficiency calculated using the data -
$\eta_f$	Energetic efficiency calculated with Eq. 3 -
$\eta_r$	Thermal recovery efficiency -
$\lambda_a$	Thermal conductivity aquifer $m^2$
$\bar{\mu}$	Viscosity of water at average of $T_i, T_g$ Pa s
$\bar{\rho}$	Density of water at average of $T_i, T_g$ $K^{-1}$
$\bar{T}_i$	Average injected temperature $^{\circ}C$
$\bar{T}_o$	Average extracted temperature $^{\circ}C$
$\pi$	Pythagoras number -
$A$	Surface area of a cylinder $m^2$
$a$	Anisotropy -
$c_w$	Volumetric heat capacity of water $Jm^{-3}K^{-1}$
$c_{aq}$	Volumetric heat capacity of saturated aquifer $Jm^{-3}K^{-1}$
$E_{in}$	Energy injected into well J
$E_{out}$	Energy extracted out of well J
$g$	Acceleration due to gravity $ms^{-2}$
$H$	Thickness aquifer $m$
$K_h$	Horizontal permeability $m^2$
$k_h$	Horizontal hydraulic conductivity $m\ day^{-1}$
$K_v$	Vertical permeability $m^2$
$k_v$	Vertical hydraulic conductivity $m\ day^{-1}$
$n$	Porosity of aquifer -
$r_h$	Hydraulic thermal radius of a well $m$
$r_{th}$	Theoretical thermal radius of a well $m$
$T_c$	Cutoff temperature $^{\circ}C$
$T_e$	Temperature of extracted water $^{\circ}C$
$T_g$	Ambient groundwater temperature $^{\circ}C$
$T_i$	Temperature of injected water $^{\circ}C$
$u$	Background groundwater flow $m\ day^{-1}$
$V_e$	Extracted water volume during one extraction period, which is in this research a single year $m^3$
$V_i$	Injected water volume during one storage period, which is in this research a single year $m^3$

#### Author contributions

David Geerts: conceptualization, methodology, software, validation, investigation, data curation, writing—original draft, and visualization. Alexandros Daniilidis: methodology, software, writing—review and editing, supervision, and funding acquisition. Gert Jan Kramer: writing—review and editing and supervision. Martin Bloemendal: methodology, software, writing—review and editing, supervision, and funding acquisition. Wen Liu: methodology, writing—review and editing, visualization, supervision, and funding acquisition.

#### Funding

This work was funded by the European Union under the Horizon Europe programme (grant no. 1011096566). Views and opinions expressed are, however, those of the author(s) only and do not necessarily reflect those of the European Union or CINEA. Neither the European Union nor CINEA can be held responsible for them.

#### Availability of data and materials

The data generated during the research is available at: [https://github.com/dayfix/DD\\_ATES](https://github.com/dayfix/DD_ATES).

## Declarations

### Competing interests

The authors declare that they have no known competing financial interests or personal relationships that could have appeared to influence the work reported in this paper.

Received: 12 December 2024 Accepted: 1 April 2025

Published online: 22 April 2025

## References

- Antony J. Design of experiments for engineers and scientists. Amsterdam: Elsevier; 2023.
- Beernink S, Hartog N, Bloemendal M, van der Meer M. Ates systems performance in practice: Analysis of operational data from ates systems in the province of utrecht, the netherlands. In Proceedings of the European Geothermal Congress, 2019.
- Beernink S, Bloemendal M, Kleinlugtenbelt R, Hartog N. Maximizing the use of aquifer thermal energy storage systems in urban areas: effects on individual system primary energy use and overall ghg emissions. *Appl Energy*. 2022;311:118587.
- Beernink S, Hartog N, Vardon PJ, Bloemendal M. Heat losses in ates systems: the impact of processes, storage geometry and temperature. *Geothermics*. 2024;117:102889.
- Birdsell DT, Adams BM, Saar MO. Minimum transmissivity and optimal well spacing and flow rate for high-temperature aquifer thermal energy storage. *Appl Energy*. 2021;289:116658.
- Bloemendal M, Hartog N. Analysis of the impact of storage conditions on the thermal recovery efficiency of low-temperature ates systems. *Geothermics*. 2018;71:306–19.
- Bloemendal M, Jaxa-Rozen M, Olsthoorn T. Methods for planning of ates systems. *Appl Energy*. 2018;216:534–57.
- Bonte M, Van Breukelen BM, Stuyfzand PJ. Environmental impacts of aquifer thermal energy storage investigated by field and laboratory experiments. *J Water Clim Change*. 2013;4(2):77–89.
- Buscheck TA. The hydrothermal analysis of aquifer thermal energy storage. Berkeley: University of California; 1984.
- Cherry JA, Freeze RA. Groundwater. Englewood Cliffs: Prentice-Hall; 1979.
- Collignon M, Klemetsdal ØS, Møyner O, Alcani   M, Rinaldi AP, Nilsen H, Lupi M. Evaluating thermal losses and storage capacity in high-temperature aquifer thermal energy storage (ht-ates) systems with well operating limits: insights from a study-case in the greater Geneva Basin, Switzerland. *Geothermics*. 2020;85:101773.
-   omaklı K, Y  ksel B,   omaklı   . Evaluation of energy and exergy losses in district heating network. *Appl Therm Eng*. 2004;24(7):1009–17.
- Cozzi L, Gould T, Bouckart S, Crow D, Kim T, Mcglade C, Olejarnik P, Wanner B, Wetzel D. World energy outlook 2020. IEA: Paris. France. 2020; 2050:1–461.
- Daniilidis A, Mindel JE, De Oliveira Filho F, Guglielmetti L. Techno-economic assessment and operational co2 emissions of high-temperature aquifer thermal energy storage (ht-ates) using demand-driven and subsurface-constrained dimensioning. *Energy*. 2022;249:123682.
- Doughty C, Hellstr  m G, Tsang CF, Claesson J. A dimensionless parameter approach to the thermal behavior of an aquifer thermal energy storage system. *Water Resour Res*. 1982;18(3):571–87.
- Drijver B, van Aarssen M, Zwart BD. High-temperature aquifer thermal energy storage (ht-ates): sustainable and multi-usable. Proceedings of the Innstock. 2012; 1–10.
- Drijver B, Bakema G, Oerlemans P. State of the art of ht-ates in the netherlands. In European Geothermal Congress: Proceedings. Netherlands: Den Haag; 2019.
- Duijff R, Bloemendal M, Bakker M. Interaction effects between aquifer thermal energy storage systems. *Groundwater*. 2023;61(2):173–82.
- Fenwick D, Scheidt C, Caers J. Quantifying asymmetric parameter interactions in sensitivity analysis: application to reservoir modeling. *Math Geosci*. 2014;46:493–511.
- Fleuchaus P, Sch  ppler S, Bloemendal M, Guglielmetti L, Opel O, Blum P. Risk analysis of high-temperature aquifer thermal energy storage (ht-ates). *Renew Sustain Energy Rev*. 2020;133:110153.
- Gao H, Zhou D, Tatmir A, Li K, Ganzer L, Jaeger P, Brenner G, Sauter M. Estimation of recovery efficiency in high-temperature aquifer thermal energy storage considering buoyancy flow. *Water Resour Res*. 2024;60(11):e2024WR037491.
- Geerts D, Daniilidis A, Liu W. A fast and accurate data-driven model for estimating the production temperature of high-temperature aquifer thermal energy storage. *Under Rev*. 2025.
- Heldt S, Beyer C, Bauer S. Uncertainty assessment of thermal recovery and subsurface temperature changes induced by high-temperature aquifer thermal energy storage (ht-ates): a case study. *Geothermics*. 2024;122:103086.
- Hermans T, Nguyen F, Klepikova M, Dassargues A, Caers J. Uncertainty quantification of medium-term heat storage from short-term geophysical experiments using Bayesian evidential learning. *Water Resour Res*. 2018;54(4):2931–48.
- Hodson TO. Root mean square error (rmse) or mean absolute error (mae): When to use them or not. *Geosci Model Dev Discuss*. 2022;2022:1–10.
- Holmslykke HD, Kj  ller C. Reactive transport modelling of potential near-well mineralogical changes during seasonal heat storage (ht-ates) in Danish geothermal reservoirs. *J Energy Storage*. 2023;72:108653.
- IEA, "Space heating," IEA, Tech Rep. 2023. <https://www.iea.org/reports/space-heating>
- Langevin CD. Modeling axisymmetric flow and transport. *Groundwater*. 2008;46(4):579–90.
- Mindel JE, Alt-Epping P, Les Landes AA, Beernink S, Birdsell DT, Bloemendal M, Hamm V, Lopez S, Maragna C, Nielsen CM, et al. Benchmark study of simulators for thermo-hydraulic modelling of low enthalpy geothermal processes. *Geothermics*. 2021;96:102130.

- Naber N, Dehens J. Update kentallen installaties vesta mais. CE Delft Tech Rep. 2022. [https://ce.nl/wp-content/uploads/2023/03/CE\\_Delft\\_210348\\_Update\\_kentallen\\_installaties\\_Vesta\\_MAIS\\_Def.pdf](https://ce.nl/wp-content/uploads/2023/03/CE_Delft_210348_Update_kentallen_installaties_Vesta_MAIS_Def.pdf). Accessed 28 Nov 2024
- Opel O, Strodel N, Werner K, Geffken J, Tribel A, Ruck W. Climate-neutral and sustainable campus Leuphana University of Lüneburg. *Energy*. 2017;141:2628–39.
- Perzan Z, Babey T, Caers J, Bargar J, Maher K. Local and global sensitivity analysis of a reactive transport model simulating floodplain redox cycling. *Water Resour Res*. 2021;57(12):e2021WR029723.
- Ranganathan A. The levenberg-marquardt algorithm. *Tutorial LM Algorithm*. 2004;11(1):101–10.
- Rijksoverheid. Mijnbouwwet. 2023. <https://wetten.overheid.nl/BWBR0014168/2023-07-01>
- Sanner B, Knoblich K. Advantages and problems of high temperature underground thermal energy storage. *Bull d'Hydrogéol*. 1999;17:341–8.
- Schout G, Drijver B, Gutierrez-Neri M, Schotting R. Analysis of recovery efficiency in high-temperature aquifer thermal energy storage: a Rayleigh-based method. *Hydrogeol J*. 2014;22(1):281.
- Sheldon HA, Wilkins A, Green CP. Recovery efficiency in high-temperature aquifer thermal energy storage systems. *Geothermics*. 2021;96:102173.
- Silvestri V, Crosta G, Prevati A, Frattini P, Bloemendal M. Uni-directional ates in high groundwater flow aquifers. *Geothermics*. 2025;125:103152.
- Sommer W, Valstar J, van Gaans P, Grotenhuis T, Rijnaarts H. The impact of aquifer heterogeneity on the performance of aquifer thermal energy storage. *Water Resour Res*. 2013;49(12):8128–38.
- Stemmler R, Hammer V, Blum P, Menberg K. Potential of low-temperature aquifer thermal energy storage (lt-ates) in Germany. *Geotherm Energy*. 2022;10(1):1–25.
- Tang DW, Rijnaarts HH. Dimensionless thermal efficiency analysis for aquifer thermal energy storage. *Water Resour Res*. 2023;59(11):e2023WR035797.
- Todorov O, Alanne K, Virtanen M, Kosonen R. Aquifer thermal energy storage (ates) for district heating and cooling: a novel modeling approach applied in a case study of a Finnish urban district. *Energies*. 2020;13(10):2478.
- van Loon L, van der Heide K. High-temperature ates at the university of Utrecht, The Netherlands. *SAE Techn Paper Tech Rep*. 1992. <https://doi.org/10.4271/929053>.
- van Lopik JH, Hartog N, Zaadnoordijk WJ, et al. The use of salinity contrast for density difference compensation to improve the thermal recovery efficiency in high-temperature aquifer thermal energy storage systems. *Hydrogeol J*. 2016;24(5):1255–1271.
- van der Roest E, Beernink S, Hartog N, van der Hoek JP, Bloemendal M. Towards sustainable heat supply with decentralized multi-energy systems by integration of subsurface seasonal heat storage. *Energies*. 2021;14(23):7958.
- Virtanen P, Gommers R, Oliphant TE, Haberland M, Reddy T, Cournapeau D, Burovski E, Peterson P, Weckesser W, Bright J, van der Walt SJ, Brett M, Wilson J, Millman KJ, Mayorov N, Nelson ARJ, Jones E, Kern R, Larson E, Carey CJ, Polat İ, Feng Y, Moore EW, VanderPlas J, Laxalde D, Perktold J, Cimrman R, Henriksen I, Quintero EA, Harris CR, Archibald AM, Ribeiro AH, Pedregosa F, van Mulbregt P, SciPy 1.0 Contributors. *SciPy 1.0: fundamental algorithms for scientific computing in python*. *Nat Methods*. 2020;17:261–72.
- Visser PW, Kooi H, Stuyfzand PJ. The thermal impact of aquifer thermal energy storage (ates) systems: a case study in the Netherlands, combining monitoring and modeling. *Hydrogeol J*. 2015;23(3):507.
- Werner S. International review of district heating and cooling. *Energy*. 2017;137:617–31.
- Ziellesny A. From curve fitting to machine learning. Berlin: Springer; 2011. p. 18.

## Publisher's Note

Springer Nature remains neutral with regard to jurisdictional claims in published maps and institutional affiliations.